Title: Impact of seismic image quality on fault interpretation uncertainty

Authors:

Juan ALCALDE[1,2] (juan.alcalde@abdn.ac.uk). Tel: +44 (0) 1224273879 (Corresponding author)

Clare E. BOND[1] (clare.bond@abdn.ac.uk). Tel: +44 (0) 1224273492

Gareth JOHNSON[2] (g.johnson@ed.ac.uk). Tel: +44 (0) 1316507010

Jennifer F. ELLIS[3] (ellisj11@cardiff.ac.uk). Tel: +44 (0) 7903262934

Robert W. H. BUTLER[1] (rob.butler@abdn.ac.uk). Tel: +44 (0) 1224273452

[1]Geology and Petroleum Geology, University of Aberdeen, School of Geosciences, Kings College, Aberdeen, AB24 3UE, UK.

[2]School of GeoSciences, University of Edinburgh, West Mains Road, Edinburgh, EH9 3FE, UK.

[3]Midland Valley Exploration Ltd, 2 West Regent Street, Glasgow, G2 1RW, UK. Current address: - Cardiff University School of Earth and Ocean Sciences, Main Building, Park Pl, Cardiff, CF10 3AT, UK.

Abstract

Uncertainty in the geological interpretation of a seismic image is affected by image quality. Using quantitative image analysis techniques we have mapped differences in image contrast and reflection continuity for two different representations of the same greyscale seismic image, one in two-way-time (TWT) and one in depth. The contrast and reflection continuity of the depth image is lower than that of the TWT image. We compare the results of 196 interpretations of a single fault contained in the seismic with the image quality. Low contrast and continuity areas correspond to a greater range of interpreted fault geometries, resulting in a broader spread of fault interpretations in the depth image. Subtle differences in interpreted fault geometries introduce changes in fault characteristics (e.g., throw, heave) that are critical for understanding crustal and lithospheric processes. Seismic image quality impacts interpretation certainty, as evidenced by the increased range in fault interpretations. Quantitative assessments of image quality could inform: 1) whether model based interpretation (e.g. fault geometry prediction at depth) is more robust than a subjective interpretation, and 2) uncertainty assessments of fault interpretations used to predict tectonic processes such as crustal extension.

1. Introduction

Interpreting seismic reflection data is the principal approach for obtaining a detailed understanding of the geological structure of the subsurface. Central to these endeavours is the ability to trace faults. The resulting interpretations of fault patterns are used to infer a wide variety of tectonic properties – for example: estimations of upper crustal stretching during lithospheric extension (e.g. Kusznir and Karner 2007), kinematic connectivity and stretching directions (e.g. Baudon and Cratwright, 2008); and polyphase reactivation and inversion (e.g. Underhill and Paterson, 1998; Badley and Backshall, 1989). Fault interpretations are important components in the prediction of hydrocarbon reservoir volumes in structural traps, and in forecasting the integrity and performance for structurally complex reservoirs (e.g. Richards et al., 2015; Yielding, 2015; Wood et al., 2015; Freeman et al., 2015). However, in publications, faults are commonly shown as single, deterministic interpretations – even though there are uncertainties in these seismic interpretations that will

impact on the application of the interpretation. A single seismic image can comprise a range of interpretations with intrinsic probabilities (Bond et al., 2007; Hardy, 2015). Despite the importance of fault interpretations, remarkably few publications or indeed training materials explain how faults are interpreted on seismic reflection profiles, nor discuss the uncertainties in the interpretations. Here we explore how image quality impacts fault interpretation, using outputs from an interpretation exercise.

Faults may be characterized as quasi-planar features that offset geological markers. It is rare that the fault surfaces themselves generate seismic reflections. Therefore, on seismic images, fault geometries are established chiefly by linking the terminations of stratal reflectors. (e.g. Bahorich and Farmer, 1995). However, there are many other explanations for reflector termination, some geophysical (e.g., noise, processing effects, anomalous changes in velocity), some geological (e.g. depositional facies changes, channels, unconformities), that are not always easy to distinguish, so there are ambiguities in fault interpretation. Subtle differences in fault interpretation introduce changes in the geometric characteristics of the faults (e.g., throw, heave), with for example impact on the determination of stretching factors for sedimentary basins. In basins that are in a late stage of being explored, 3D seismic data is often employed because it generally provides a higher spatial resolution and geometric continuity compared with even closely-spaced grids of 2D seismic profiles (Cartwright and Huuse, 2005; Gao, 2009), but significant uncertainty in structural interpretation can still exist. Regardless of the development of 3D seismic methods, 2D data continues to underpin regional tectonic studies and frontier basin exploration (e.g. Platt and Philip, 1995; Thomson and Underhill, 1999; Gabrielsen et al., 2013). Much of the understanding of fault geometry is based on heritage 2D data from the 1980s (e.g. Freeman et al., 1990), even if enhanced by subsequent 3D studies (e.g. Cartwright and Huuse, 2005). Furthermore, training materials in fault interpretation (e.g., Shaw et al. 2005), as well as knowledge-sharing resources (i.e., books and articles), are chiefly two-dimensional, presented in paper or on computer screen. In summary, 2D interpretation is a fundamental and important part of most seismic interpretations irrespective of whether the data is available as 2D lines or 3D volumes. In spite of its importance, the impression given by these training materials and by the expert community is that fault interpretation in seismic imagery is routine and carries little uncertainty.

2. How do we see seismic images

Seismic data is viewed and interpreted manually as an image. There are a number of visual factors that affect how we perceive objects, including colour, intensity, hue or perspective (e.g. Froner et al., 2013). These factors determine the saliency of the different elements that form an image. Visual saliency refers to the distinctiveness of an element, i.e., the capacity to draw the attention of the viewer (e.g., Kadir and Brady, 2001; Kim et al., 2010), and is mainly dependent on its distinction from nearby elements (Cheng et al., 2011). Visual saliency produces biases in favour of the most prominent elements (Reynolds and Desimone, 2003), and hence influences interpretation. As such, increasing image contrast enhances differences between prominent elements in an image (Reynolds and Desimone, 2003).

Classically, seismic imagery is presented as a grey-scale, although it is now commonly visualised in colour, using either linear or non-linear colour spectrums (Froner et al., 2013). Non-linear colour spectrums are often used to highlight maximum and minimum amplitude reflectors. When employing an 8-bit black and white computer render, image contrast represents the range in amplitude of seismic reflection data as 256 pixels in different shades of grey. Similarly, reflection continuity (the saliency of a reflector) is represented by adjoining pixels of the same, or a similar, shade of grey. Modern 64-bit computers can display images in millions of grey or colour shades. However, human perception of images presented in grey scale is poorly understood and an active area of research (Song et al., 2010; Radonjic et al., 2011). Our aim is to test if even “simple” 8-bit grey scale visualisations of seismic images of different quality have an impact on interpretation outcome.

3. Interpretation Experiment

We presented a seismic image to 196 interpreters in a controlled experiment, and compared their interpretations of a major fault in the seismic image, with the image quality. The seismic reflection image from the Gulf of Suez (Fig. 1) was presented either in two-way travel time (TWT, Fig. 1a) - 70 subjects, 36% of the

90 interpretations - or in depth domain (Fig. 1b) - 126 subjects, 64% of the interpretations (Figs. 1c and 1d,
91 respectively). The participants were asked to "interpret the major fault crossing the section and the main
92 sedimentary horizons as deep as they could". They were also asked to provide further annotation and/or
93 sketching to support their interpretations. In this contribution, we focus purely on the fault interpretations as
94 drawn by the participants on the seismic image. Participants had up to 30 minutes to complete their
95 interpretations. The interpreters' proficiencies were highly diverse, and their experience ranged from
96 unexperienced students to interpretation specialists with more than 30 years of experience.

97 The seismic section used in the experiment is a 31 km long and extended to 6 s TWT (Fig. 1a). The
98 seismic image includes a lateral disruption of the reflections in the central part, generally interpreted as a
99 fault, but with some degree of uncertainty as to the fault's placement, geometry and extent. The TWT section
100 was converted to depth using a simple velocity model in Move™, described by Eq. (1):

101 $$Z = V_0 \frac{\left(e^{kt}-1\right)}{k} \quad (1)$$

102 where Z is the depth in metres, V_0 is the initial velocity (1500 ms^{-1}), t is one-way travel time and k is
103 the rate of change in velocity with increasing depth (0.5). The depth conversion located the bottom of the
104 section at 10.5 km depth. The depth conversion was completed on a bitmap of the seismic reflection image,
105 which linearly stretches the image. The result is a depth section with apparently lower reflectivity and contrast
106 than the original TWT image and 18 % longer, due to this stretching. With the exception of depth conversion
107 both the TWT and depth images share identical processing workflows. The actual depth conversion method
108 used is not important for our experiment; it is the difference in image quality the process creates that concerns
109 us.

110 **4. Image Analysis**

111 The image analysis undertaken focused on the pixel intensity contrast and reflection continuity
112 (referred to hereafter as "contrast" and "continuity", respectively) of the TWT and depth sections (see
113 Supplemental Figure S1). For the image analysis, each seismic image was subdivided into cells of 7.2 km
114 (length) x 1 km (depth) (1135 x 450 pixels). The area encompassing the participants' fault interpretations was

115 subdivided into smaller cells 1.6 km x 0.4 km (216 x 163 pixels), in order to provide detailed image analysis
116 information in the area of interest. For ease of comparison of our results, the seismic images are both shown
117 with a vertical scale in depth in all figures (except Fig. 1a) .

118 To analyse the image contrast we extracted grey scale distributions for the pixels in each cell for the
119 two uninterpreted images. The distributions range from pixel number 0 (black) to 255 (white): the wider these
120 distributions are (i.e. the more pixel values close to the extremes of 0 and 255), the more contrast the image
121 has; the narrower the pixel distribution, the more similar the pixel values are and thus the lower the contrast.
122 The first and third quartiles (Q_1 and Q_3) from these distributions were subtracted in order to calculate the
123 interquartile range (I_Q) of the distributions. We use the interquartile range as an analogue for visual contrast:
124 the wider the I_Q of the cell, the higher the contrast and vice versa. Each cell in the images is coloured according
125 to its I_Q value in order to display graphically the contrast analysis results.

126 To analyse the reflector continuity, the images were first converted into a binary, i.e., a black and
127 white image. This was performed using ImageJ software (Schneider et al., 2012) by setting an automatic
128 threshold level based on the histograms of the two images. This threshold divides the pixel histogram in two
129 halves, assigning black or white colour to all the pixels. As a result, the seismic wave reflections are separated
130 into isolated black bodies, corresponding to the positive amplitude reflections in this particular case, included
131 in a white background. A macro for the software ImageJ (Heilbronner and Barrett, 2013) was used to measure
132 and analyse these resultant bodies. In the analysis, the length of the major axis of each reflection is calculated,
133 using a best-fit ellipse method, and each reflection is then coloured based on this length value using a colour
134 scale.

135

136 **5. Interpretation Outcomes**

137 Interpretations of the major discontinuity of reflectors (faults) located in the middle of the seismic images
138 and related splay faults (327 elements in total) were used in the analysis. Of these elements, 116 correspond
139 to the interpretations of the TWT image (Fig. 1c) and 211 to the interpretations of the depth seismic image

(Fig. 1.d). In general, variability in fault placement position (the spread in fault interpretations) increases with depth, and this observation is more pronounced in those interpretations derived from the depth image. The difference in fault placement spread between the two images is at a maximum at 5 km depth. Below this point, the amount of interpreted faults dipping to the right is greater in the depth section (23 faults) than in the TWT section (5 faults). The effect of the difference in the populations of TWT and depth interpretations was analysed, by randomly selecting 70 of the depth interpretations for comparison with the TWT interpretation population of 70. As these were found to be similar to the full depth interpretation analysis, we conclude that population size had no effect on the results.

Quantification of the variability in fault placement for the interpretation populations were computed at nine depth markers in each seismic image (Fig. 2). At each depth marker the four quartiles and outliers positions for the fault interpretation populations were calculated (results of the analysis are shown in Fig. 2, overlaying the image analyses). The inter quartile fault range (the distance between quartile 1 and quartile 3) provides a good estimation of the fault placement spread within each of the interpretation populations at a given depth (continuous black lines in Fig. 2, created from joining the quartiles between depth markers). We use the inter quartile range of fault placement within each fault interpretation population as an indicator of fault placement uncertainty for each seismic image. The inter quartiles show that fault spread remains similar in the upper 3.5 km. From 3.5 km downwards, the inter quartile fault range in the depth image increases until, at the base of the seismic image, the inter quartile width is twice that observed in the TWT image. The increase in fault spread defined by the inter quartile trend linearly increases in the TWT image with depth. In the depth image the 1st interquartile follows a similar path to that of the TWT image, but the 3rd interquartile is more heterogeneous (wavy) and is offset to the right with respect to the 3rd interquartile line in the TWT image. Meanwhile, the outliers (dashed black lines in Fig. 2) show a similar general pattern with fault spread increasing with depth, but with a greater variability and heterogeneity. The fault placement outliers for the fault interpretations of the TWT image show a convergent trend down to 2 km in width at circa 4 km depth, before the fault placement spread increases to almost 15 km at the base of the image. The fault placement outliers from the depth interpretation show a relatively constant spread (circa 4.5 km width) down to 3 km

166 depth. Below this point, fault spread increases with depth resulting in a 15 km spread in fault interpretations
167 at the base of the seismic image. There is also a clear difference in the length of the faults interpreted. The
168 depth of the first and last point of the faults were measured, resulting in an average depth of 4.7 km and 6.6
169 km for the faults interpreted in TWT and depth, respectively.

170

171 **6. Image Quality**

172 *Image contrast*

173 Contrast in the TWT seismic image is almost three times greater than in the depth image (Fig. 1c and
174 1d). Detailed contrast analysis of both seismic images show a decrease in contrast with depth as well as higher
175 contrast to the left of the fault location as compared to the right (Fig. 2a and 2b). There is a visible spatial
176 association between lower contrast areas in the seismic imagery and a larger spread in fault placement
177 certainty (Fig. 2a and 2b). This effect is especially visible in areas with very low I_Q, which correspond to
178 maximum fault placement dispersion (i.e., dark green and blue colours in Fig. 2b). In the TWT seismic image,
179 the I_Q values remain moderate when compared to the depth image. This may account for the smaller inter
180 quartile range in fault placement in the lower half of the TWT image in comparison to the depth image (Fig.
181 2b).

182 The outlier fault interpretations (dashed lines in figure 2a and 2b) are also likely to have been affected
183 by image contrast; indications of this influence can be seen in figure 2a where the left outlier line follows the
184 yellow/green pixel contrast binning boundary at 2.5 to 7 km depth. The convexity of the right outlier towards
185 the third quartile at 3.5 km depth and circa 15 km distance along the TWT seismic image was associated with
186 the existence of higher contrast cells (yellow colours) in comparison to surrounding cells at this point (Fig. 2a).

187 *Reflection continuity*

188 Reflection continuity decreases with depth in the seismic images and to the right of the main fault.
189 Reflection continuity is, on average, 63% smaller in the depth image than in the TWT image (Fig. 2c and 2d).
190 We associate this dramatic reduction in continuity to the decrease in contrast as a result of the depth
191 conversion. Interpreted faults tend to cross areas with lower reflection continuity. This is not surprising, as

faults that cut and disrupt rock layers with the same reflective physical properties would create low reflection continuity. The fault interpretations coincide with where reflectors from the left join those coming from the right, at approximately 13-16 km along the seismic image, at circa 6 km depth. The Q_3 of the TWT interpretations follow this boundary. In the depth seismic image this joining of reflectors is less clear (potentially due to the lack of reflectivity/continuity), and the 3rd quartile is more variable, especially in the deeper part below 5 km. The greater amount of faults dipping to the right below 5 km depth in the depth image can be explained by a lack of reflection continuity at distances along the section line greater than 13 km, and 5km depth (Fig. 2d). In the TWT image, right-dipping faults have to be interpreted crossing strong, continuous reflections below 5 km, and most right -dipping fault interpretations stop at a shallower depths (from 17 fault interpretations at 3 km depth to only 5 at 5 km depth). In the depth image, the reflections are more discontinuous and fault interpretations continue to greater depths. The extent of the outliers also seems to be affected by reflection continuity. In the TWT seismic image for example, the right outlier line, coincides with a break in reflection continuity between 4 -10 km depth (Fig. 2c); in the depth image, the right outlier stays to the left of a package with more continuous horizontal reflections, located at 2.5 to 5.5 km depth (Fig. 2d).

Combined image analysis

The analysis of contrast and continuity highlighted spatial associations between image quality and fault interpretation (Fig. 2a to 2d). In reality the image, as viewed by the interpreter, is the result of combining both contrast and continuity. In an attempt to merge the results of the contrast and continuity analyses, the continuity analysis was converted into a cell model, based on the contrast grid. This conversion assigned the maximum continuity value contained within a cell, to each cell in the grid. To merge the analyses, cells in the new continuity cell model were multiplied with the values from the respective cells from the contrast analysis. In spite of the potential different impact of the two parameters on the interpreters and their relative co-dependency (i.e., enhancing the contrast can enhance the continuity), creating a combined parameter provides a general visualisation of image quality. The results were normalized by representing the maximum

value as 100 and the minimum as zero. The resulting merged models for the depth converted TWT and depth images are shown in Figures 2e and f.

There is a diffuse horizontal boundary in the merged values in the TWT image at circa 4.5 km depth (Fig. 2e), marking a change from 'green' and hotter colours at shallower levels to lower 'blue' values as depth increases. This 4.5 km depth marks the point at which the distance between the 1st and 3rd quartiles increases from 523 m to more than double (1234 m) at the bottom of the section. This boundary also coincides with the average depth of the interpreted TWT faults, suggesting that it marks a clear increment in the uncertainty of the image for interpretation. Faults are interpreted until a deeper point in the depth image, potentially because this boundary in image quality is less perceptible. The positions of the outlier interpretations show a greater change, from a narrow converging spread to divergent with the spread increasing with depth. In the case of the depth image (Fig. 2f) this boundary is less noticeable, possibly due to the overall low values, poor image quality, although fault spread does increase with depth below 4.5 km. The results suggest that there may be a contrast and continuity threshold within the seismic images beyond which the fault interpretations are almost unconstrained by the data.

7. Impact on Interpretation

The experiment outlined above shows that image contrast and the continuity of features both impact on the interpretation outcome of the seismic imagery. Interpreters are less prone to cross stratal reflections if they are "strong" (i.e., high contrast and high continuity) and where reflections are "weak", uncertainty in interpretation increases. In general, enhancing image contrast helps to constrain the interpretation, as seen in the TWT image where image contrast is three times that of the depth image and the fault placement population shows a narrower spread and shorter faults. A similar pattern is observed for reflection continuity, where high reflection continuity also results in a narrower fault placement spread and shorter fault interpretations. The differences in fault spread observed determine predicted fault heave; resulting, for example in regional sections, in significant differences in crustal stretching predictions. Further work to assess

242 the relative contributions of contrast and continuity to visual image quality to create a single weighted
243 parameter would provide a fully quantified visualisation of image quality.

244 The two images were presented in different domains (TWT and depth), resulting in an 18% longer
245 vertical scale in the depth image which could have changed the perception of the fault geometries to
246 interpreters. However, our correlations suggest that image quality had the major influence on interpretation
247 choice. We note that the average depth of the faults interpreted in the TWT image coincides with a boundary
248 in depreciating image quality in the combined analysis. Although our results show that depth conversion
249 choices (including the method used) change seismic image quality, all image manipulations have the potential
250 to change interpretation outcomes. We therefore need to better understand image perception so that such
251 image manipulations do not arbitrarily influence or bias interpretation outcome.

252 For a fixed binary threshold, image contrast and continuity are associated parameters, so increasing
253 image contrast can artificially increase continuity. This correlation causes issues in determining the best
254 methods for enhancing imagery in order to maximise interpretation effectiveness. It also has impacts on the
255 processing of seismic data and the model chosen to create an image. Initial processing models generally
256 assume a sub-horizontal, sub-parallel reflector stratigraphy with minimal disruption. Thus, they enhance
257 reflector continuity. Our results, albeit based on TWT and depth imagery rather than different processing
258 models, show that reflector continuity is spatially related to fault placement certainty. The processing of strong
259 reflector continuity in seismic image data may result in greater constraint, or certainty, in fault placement than
260 is warranted by the original data. Processing models must therefore be chosen carefully and interaction
261 between the processor and the interpreter encouraged.

262 The results of the image analysis imply that there is a threshold at which seismic image data is too
263 indeterminate (i.e., not enough contrast or continuity) to drive the interpretation. Quantitative image analysis
264 could be used to determine the extent of an interpretation that is data-supported and areas that are more
265 subjective. To create interpretations for under-constrained problems, reference models can be employed such
266 as of fold or fault shape. These reference models can be based on mechanical and geometric rules: e.g. angle

of faulting, based on Andersonian mechanics (Anderson, 1905, 1951); or depth to detachment for faults (Chamberlin, 1910), based on mass balance principles (Dahlstrom, 1969; Elliot, 1983). Indeed, Bond et al. (2012) show that in areas of poor constraint, simple geological reasoning and reconstruction analysis can be used to reduce interpretation uncertainty. The method proposed in this work opens the door for a workflow for image quality assessment to indicate those occasions when model-based interpretation (e.g. fault geometry prediction at depth) maybe more robust than the subjective fault interpretation of a geologist. Of course, these two approaches are complimentary: image analysis may aid the interpreter in determining when geometric modelling may be useful, and when interpretation uncertainty and therefore potential risk is high.

Even in the advent of more complex visualisation through computing and screen technology, including the use of colour and a greater pixel spectrum, interpretation uncertainty is determined by the quality of a seismic image. Understanding the impact of image quality on seismic interpretation, using an 8 bit grey scale image, provides a basis from which to investigate more complex aspects of visual perception including colour and luminescence. This work requires interdisciplinary research with cognitive scientists, neurologists and others to fully understand how best to represent seismic imagery to maximise interpretation efforts.

A key finding of our experiments is that there are significant variations in the interpretation of fault geometries as depth increases in the section. This reflects the decay in image quality with depth. This uncertainty may be important – for example in picking the hanging-wall cut-offs of stratal reflectors on normal faults to correlate with those in the footwall that are otherwise well-imaged. This, in turn, influences determinations of fault heave – information that is critical for constructing maps that show fault linkages in sedimentary basins and for determining net extension of the upper crust. These inherent uncertainties arising from image quality are generally unreported in larger-scale studies of fault patterns. Therefore, the maps and net extension calculations used in many tectonic studies carry unknown errors.

REFERENCES

Anderson, E. M. 1950. The dynamics of faulting. Transactions of the Edinburgh Geological Society, 8, 387–402.

292 Anderson, E. M. 1951. The Dynamics of Faulting and Dyke Formation with Application to Britain. 2nd edn.
293 Oliver and Boyd, Edinburgh. Ashcroft, W. (2011). A petroleum geologist's guide to seismic reflection.
294 John Wiley and Sons, 157 pp.

295 Bahorich, M., and Farmer, S. 1995. 3-D seismic discontinuity for faults and stratigraphic features: The
296 coherence cube. The leading edge, 14(10), 1053-1058.

297 Badley, M.E. and Backshall, L.C. 1989. Inversion, reactivated faults and related structures: seismic examples
298 from the southern North Sea. Geological Society, London, Special Publications, 44(1), pp.201-219.

299 Baudon, C. and Cartwright, J. 2008. The kinematics of reactivation of normal faults using high resolution throw
300 mapping. Journal of Structural Geology, 30(8), pp.1072-1084.

301 Bond, C. E., Gibbs, a. D., Shipton, Z. K., and Jones, S. 2007. What do you think this is? "Conceptual uncertainty"
302 in geoscience interpretation. GSA Today, 17(11), 4.

303 Bond, C. E., Lunn, R. J., Shipton, Z. K., and Lunn, A. D. 2012. What makes an expert effective at interpreting
304 seismic images? Geology, 40(1), 75–78.

305 Cartwright, J., and Huuse, M. 2005. 3D seismic technology: The geological "Hubble." Basin Research, 17(1), 1–
306 20.

307 Chamberlin, R.T. 1910. The Appalachian folds of central Pennsylvania. Journal of Geology 18, 228–251.

308 Cheng, M.-M., Zhang, G.-X., Mitra, N.J., Huang, X., Hu, S.-M. 2011. Global contrast based salient region
309 detection. Proceedings of the IEEE Computer Society Conference on Computer Vision and Pattern
310 Recognition, art. no. 5995344, pp. 409-416.

311 Dahlstrom, C.D.A. 1969. Balanced cross sections. Canadian Journal of Earth Sciences 6, 743–757.

312 Elliott, D. 1983. The construction of balanced cross-sections. Journal of Structural Geology v5, 101.

313 Froner, B., Purves, S.J., Lowell, J., Henderson, J. 2013. Perception of visual information: The role of colour in
314 seismic interpretation. First Break, 31 (4), pp. 29-34.

315 Freeman, B., Yielding, G., and Badley, M. 1990. Fault correlation during seismic interpretation. First Break. 8,
316 Issue 3, pp. 87-95.

317 Freeman, B., Quinn, D.J., Dillon, C.G., Arnhild, M. and Jaarsma, B. 2015. Predicting subseismic fracture density
318 and orientation in the Gorm Field, Danish North Sea. Geological Society, London, Special Publications,
319 421, pp.SP421-9.

320 Gabrielsen, P.T., Abrahamson, P., Panzner, M., Fanavoll, S. and Ellingsrud, S. 2013. Exploring frontier areas
321 using 2D seismic and 3D CSEM data, as exemplified by multi-client data over the Skrugard and Havis
322 discoveries in the Barents Sea. First Break, 31(1).

323 Gao, D. 2009. 3D seismic volume visualization and interpretation: An integrated workflow with case studies.
324 Geophysics, 74(1), W1.

325 Hardy, S. 2015. "The Devil truly is in the detail. A cautionary note on computational determinism: Implications
326 for structural geology numerical codes and interpretation of their results." Interpretation, 3(4), SAA29-
327 SAA35.

328 Heilbronner, R., and Barrett, S. 2013. Image analysis in earth sciences: microstructures and textures of earth
329 materials (Vol. 129). Springer Science & Business Media.

330 Kadir, T., Brady, M. 2010. Saliency, scale and image description. International Journal of Computer Vision, 45
331 (2), pp. 83-105.

332 Kim, Y., Varshney, A., Jacobs, D. W., and Guimbretiere, F. 2010. Mesh saliency and human eye fixations. ACM
333 Trans. Appl. Percept. 7, 2, Article 12, February 2010, 13 pages.

334 Kusznir, N.J. and Karner, G.D. 2007. Continental lithospheric thinning and breakup in response to upwelling
335 divergent mantle flow: application to the Woodlark, Newfoundland and Iberia margins. Geological
336 Society, London, Special Publications, 282(1), pp.389-419.

337 Platt, N.H. and Philip, P.R. 1995. Structure of the southern Falkland Islands continental shelf: initial results from
338 new seismic data. Marine and Petroleum Geology, 12(7), pp.759-771.

339 Radonjic, A., Allred, S. R., Gilchrist, A. L., and Brainard, D. H. 2011. The Dynamic Range of Human Lightness
340 Perception. Current Biology 21 (22): 1931–36.

341 Reynolds, J. H., and Desimone, R. 2003. Interacting Roles of Attention and Visual Salience in V4. Neuron,
342 Volume 37, Issue 5, pp. 853-863

343 Richards, F.L., Richardson, N.J., Bond, C.E. and Cowgill, M. 2015. Interpretational variability of structural traps:
344 implications for exploration risk and volume uncertainty. Geological Society, London, Special
345 Publications, 421(1), pp.7-27.

346 Schneider, C.A., Rasband, W.S., Eliceiri, K.W. 2012. NIH Image to ImageJ: 25 years of image analysis. Nature
347 Methods 9, 671-675, 2012.

348 Shaw, J.H., Connors, C. and Suppe, J. (eds). 2005. Seismic interpretation of contractional fault-related folded.
349 AAPG Seismic Atlas – Studies in Geology v 53, pp. 156.

350 Song, M., Tao, D., Chen, C., Li, X., and Chen, C. W. 2010. Color to Gray: Visual Cue Preservation. IEEE
351 Transactions on Pattern Analysis and Machine Intelligence 32 (9): 1537–52.

352 Thomson, K. and Underhill, J.R. 1999. Frontier exploration in the South Atlantic: structural prospectivity in the
353 North Falkland Basin. AAPG bulletin, 83(5), pp.778-797.

354 Underhill, J.R., and Paterson, S. 1998. Genesis of tectonic inversion structures: Seismic evidence for the
355 development of key structures along the Purbeck-Isle of Wight Disturbance. Journal of the Geological
356 Society, 155 (6), pp. 975-992.

357 Wood, A.M., Paton, D.A. and Collier, R.E.L. 2015. The missing complexity in seismically imaged normal faults:
358 what are the implications for geometry and production response?. Geological Society, London, Special
359 Publications, 421(1), pp.213-230.

360 Yielding, G. 2015. Trapping of buoyant fluids in fault-bound structures. Geological Society, London, Special
361 Publications, 421, pp.SP421-3.

362

ACKNOWLEDGEMENTS

BP/GUPCO are acknowledged for providing data from the Gulf of Suez. The authors acknowledge the support of MVE and use of Move software 2015.2 for this work. Ruediger Kilian is acknowledged for his kind help with the ImageJ code. Dr Juan Alcalde is funded by NERC grant NE/M007251/1, on interpretational uncertainy. The work could not have been completed without the support of individuals within the geoscience community who took part in the interpretation experiment.

Figure 1

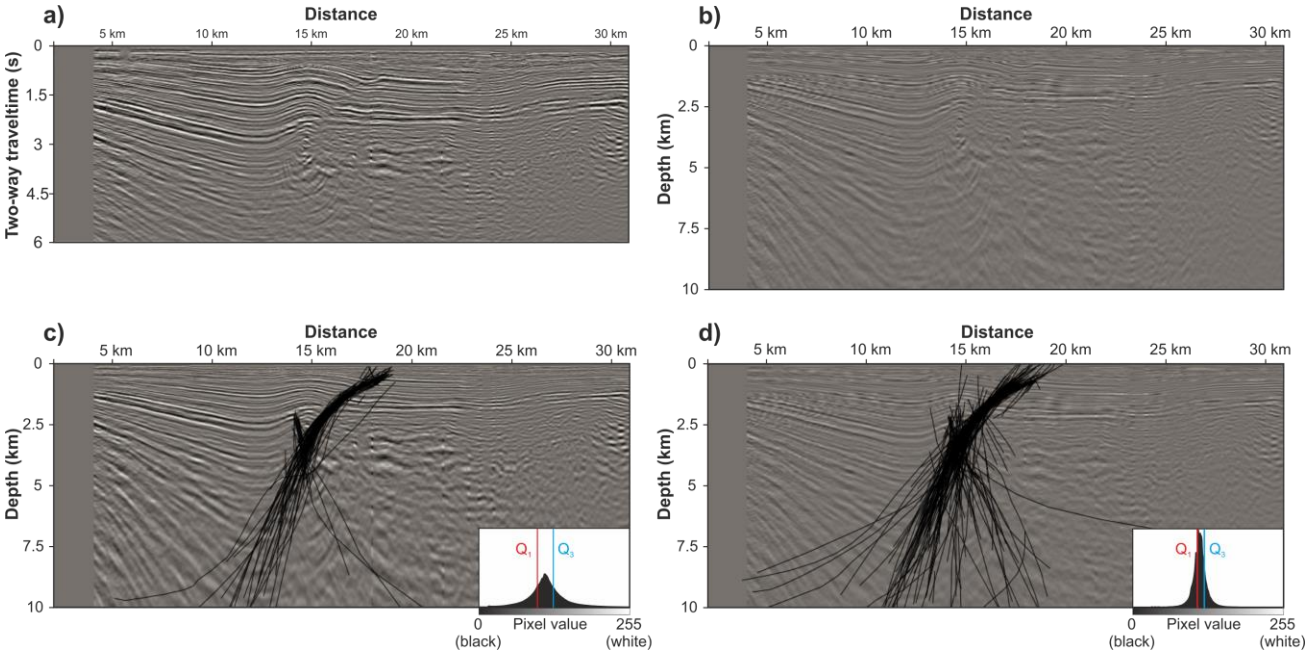
a)
Distance
5 km
10 km
15 km
20 km
25 km
30 km
Two-way traveltime (s)
0
1.5
3
4.5
6
b)
Distance
Depth (km)
0
2.5
5
7.5
10
c)
Distance
Depth (km)
Q_1
Q_3
0
(black)
Pixel value
255
(white)
d)
Distance
Depth (km)
Q_1
Q_3
0
(black)
Pixel value
255
(white)

Figure 2

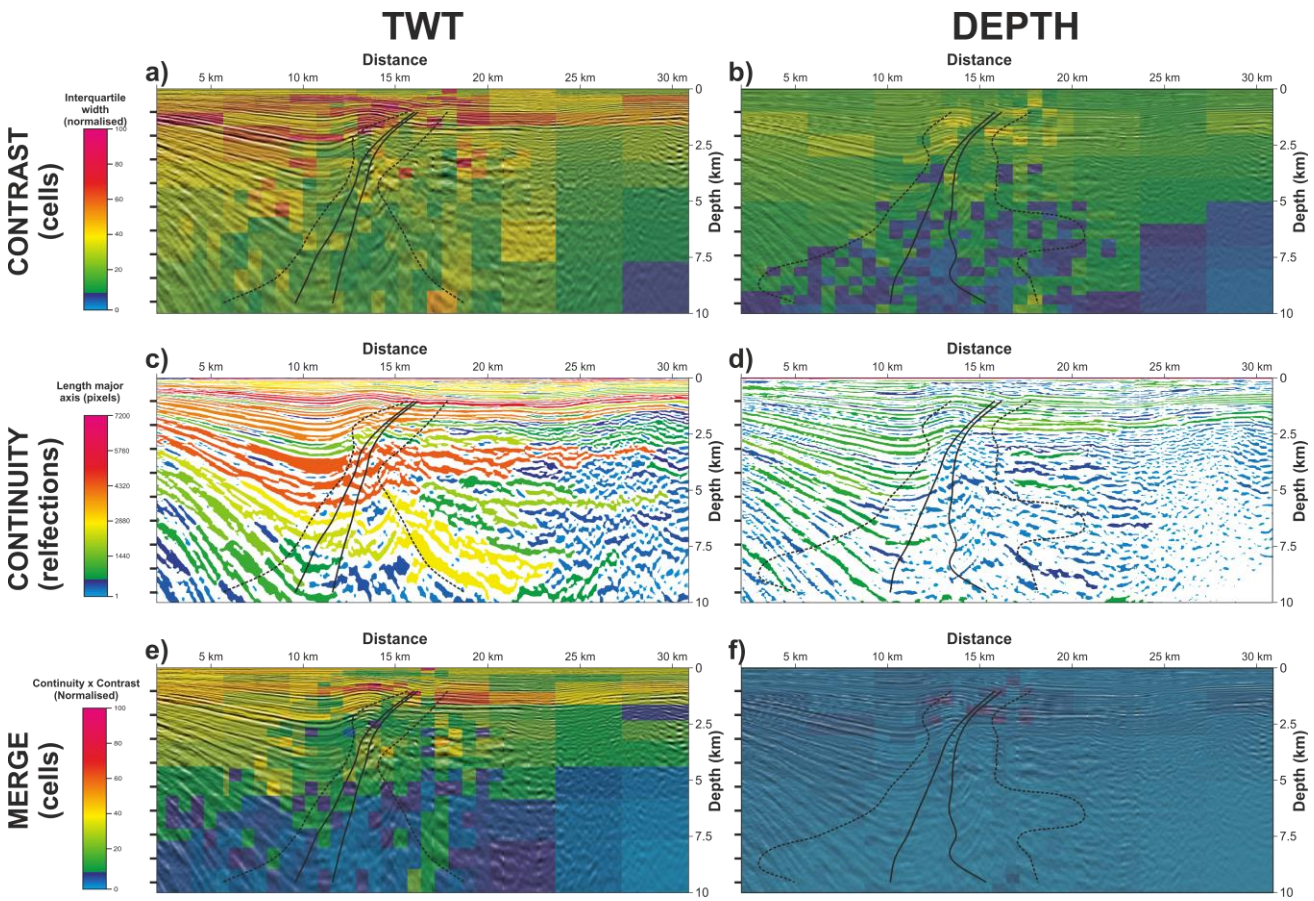
TWT
DEPTH
a)
b)
c)
d)
e)
f)
Distance
5 km
10 km
15 km
20 km
25 km
30 km
Depth (km)
0
2.5
5
7.5
10
CONTRAST (cells)
Interquartile width (normalised)
CONTINUITY (relfections)
Length major axis (pixels)
MERGE (cells)
Continuity x Contrast (Normalised)

Supplementary Figure 1

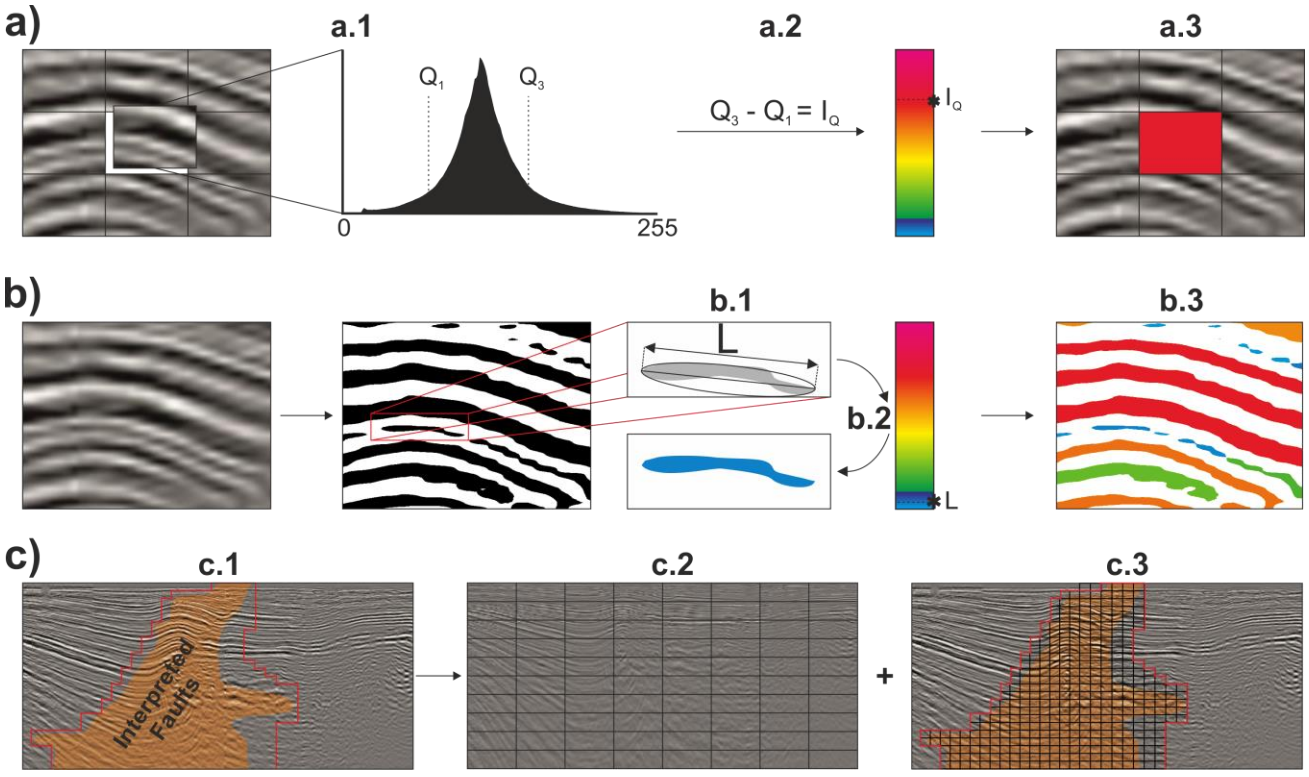

Figure captions

Figure 1: seismic sections used in the interpretation experiment. **(a)** Seismic section in two-way travel time (TWT). **(b)** Seismic section in depth. **(c)** and **(d)** Stacked results of the interpreted faults in TWT and depth (respectively). The figure includes the histogram of the corresponding section. In the histograms, the X-axis represents the possible grey values (from 0-black to 255-white) and the Y-axis the number of pixels found for each value. Note that the sections conserve the vertical scale in which they were presented to the participants and that the results in TWT were converted to depth, to be comparable with those interpreted in the Depth section. The sections are courtesy of BP/GRUPCO.

Figure 2: Results of the analysis carried out in the TWT (**a, c** and **e**) and Depth (**b, d** and **f**) seismic sections with the respective fault spread superimposed (outlier limits marked with dashed lines, 1^{st} and 3^{rd} quartile marked in continuous lines). **(a)** and **(b)** contrast analysis – warm colours represent high values in interquartile difference (i.e., high contrast) and cold colours represent low values (i.e., low contrast); **(c)** and **(d)** continuity analysis – reflections coloured according to the length of their major axis, with warm colours indicating long lengths (i.e., high continuity) and cold colours short length (i.e., low continuity); **(e)** and **(f)** merge of the two analysis – the results have been combined in a 1:1 relation, that is, the contrast and continuity values have been multiplied and normalised to 100. Note that the TWT results have been depth-converted for comparison (i.e., located at the same point) to the depth results. The black lines at the left side of the images mark the depths of the nine positions at which the fault placement for the interpretation populations were computed in each seismic image.

Supplementary material: Figure caption

Figure S1: Scheme of the methodology followed for the contrast **(a)** and continuity **(b)** analyses, and the areas selected for large and small cells used in the calculations (c). **(a)** The first (Q_1) and third (Q_3) quartiles are calculated from the pixel distributions of each subsection (a.1); the interquartile difference (I_Q, a.2) is calculated by subtracting Q_1 from Q_3 and the corresponding cell is coloured according to this value (a.3). **(b)** The reflections are separated and the major axis length (L) of each reflector body is calculated following a best-fit ellipse method (b.1); the reflection is coloured according to its own L value (b.2) normalized to the rest of the section (b.3). **(c)** A priority area, marked by the extent of the interpreted faults was identified (red line in c.1); all the calculations were carried out first dividing the section in large cells of 7.2 km (length) x 1 km (deep) (c.2), and then using a smaller cell size of 1.6 km x 0.4 km in the priority area (c.3).